

Heat Transport by Coherent Rayleigh-Bénard Convection

Fabian Waleffe,^{1,2} Anakewit Boonkasame,¹ and Leslie M. Smith^{1,2}

¹*Department of Mathematics, University of Wisconsin, Madison, WI 53706*

²*Department of Engineering Physics, University of Wisconsin, Madison, WI 53706**

(Dated: December 3, 2024)

Steady but generally unstable solutions of the 2D Boussinesq equations are obtained for no-slip boundary conditions and Prandtl number 7. The primary solution that bifurcates from the conduction state at Rayleigh number $Ra \approx 1708$ has been calculated up to $Ra \approx 5.10^6$ and shows heat flux $Nu \sim 0.143 Ra^{0.28}$ with a delicate spiral structure in the temperature field. Another solution that maximizes Nu over the horizontal wavenumber has been calculated up to $Ra = 10^9$ and its heat flux scales as $Nu \sim 0.115 Ra^{0.31}$ for $10^7 < Ra \leq 10^9$, quite similar to 3D turbulent data. The latter is a simple yet multi-scale coherent solution whose horizontal wavenumber scales as $0.133 Ra^{0.217}$ in that range. That optimum solution is unstable to larger scale perturbations and in particular to mean shear flows, yet it appears to be relevant as a backbone for turbulent solutions, possibly setting the scale, strength and spacing of elemental plumes.

Rayleigh-Bénard convection is the buoyancy-driven motion of a fluid contained between two horizontal plates and heated from below. It is a paradigmatic problem with a rich array of nonlinear physics from deterministic chaos [1] and period doubling [2] to pattern formation [3] and turbulence [4]. A fundamental issue is to determine how the heat flux \mathcal{H} scales with the temperature difference ΔT between the bottom and top plates. There is a critical ΔT_c such that heat transport is by conduction with $\mathcal{H} \sim \Delta T$ for $\Delta T < \Delta T_c$ but macroscopic fluid motion develops for $\Delta T > \Delta T_c$ and enhances heat transport. Bifurcations take place as ΔT is increased, leading to turbulent flow and $\mathcal{H} \sim (\Delta T)^{4/3}$ and perhaps even as high as $\mathcal{H} \sim (\Delta T)^{3/2}$. Understanding these bifurcations and the actual scaling of \mathcal{H} with ΔT have been the subjects of many experimental, theoretical and numerical studies focusing on *turbulent* convection [4]. Here, we consider *coherent* convection – non-trivial steady flows that may be the permanent form of the coherent structures (the “plumes”) permeating turbulent convection.

In Rayleigh-Bénard convection, the fluid is contained between two infinite horizontal plates and the Boussinesq approximation is made so the governing equations are

$$\frac{\partial \mathbf{v}}{\partial t} + (\mathbf{v} \cdot \nabla) \mathbf{v} + \nabla p = g \alpha_v T \hat{\mathbf{y}} + \nu \nabla^2 \mathbf{v}, \quad (1)$$

$$\frac{\partial T}{\partial t} + (\mathbf{v} \cdot \nabla) T = \kappa \nabla^2 T, \quad (2)$$

for the velocity \mathbf{v} and the temperature T . Incompressibility $\nabla \cdot \mathbf{v} = 0$ is maintained by the kinematic pressure p and $-g \hat{\mathbf{y}}$ is the constant acceleration of gravity. The fluid density is $\rho \approx \rho_0(1 - \alpha_v T)$ with $\alpha_v \geq 0$ the volumetric thermal expansion coefficient and ρ_0 a constant reference density, $\nu > 0$ is the kinematic viscosity and $\kappa > 0$ the thermal diffusivity. The bottom plate temperature is fixed at $\Delta T/2$ and the upper plate is at $-\Delta T/2$. The conduction state is the solution $\mathbf{v} = 0$, $T = -y \Delta T/H$ to (1) and (2), with $-h \leq y \leq h = H/2$. This is a steady solution for all values of the parameters, but Rayleigh showed

that it is linearly unstable when the *Rayleigh* number

$$Ra = \frac{g \alpha_v \Delta T H^3}{\nu \kappa} \quad (3)$$

is larger than a critical value Ra_c , independent of the *Prandtl* number $Pr = \nu/\kappa$. We consider no-slip boundary conditions for which $Ra_c \approx 1708$ for horizontal wavenumber $\alpha_c = 3.116/H$ [5]. Convection develops and enhances heat transport for $Ra > Ra_c$. For statistically steady solutions, integration of (2) gives

$$\mathcal{H} = -\kappa \left. \frac{d\bar{T}}{dy} \right|_{y=\pm h} = \kappa \frac{\Delta T}{H} + \langle vT \rangle \quad (4)$$

for the heat flux [6], [7], where $v = \hat{\mathbf{y}} \cdot \mathbf{v}$ is the vertical velocity with $\bar{*}$ and $\langle * \rangle$ denoting horizontal and domain averages, respectively.

We non-dimensionalize the equations using $\Delta T/2$, h , $\tau = \sqrt{h/g'}$, and $V = \sqrt{g'h}$, as our temperature, length, time and speed scales, respectively, where $g' = g \alpha_v \Delta T/2$ is the reduced gravity. A physical picture for these scalings is that of a fluid at temperature $T = 0$, with cold plumes at temperature $-\Delta T/2$ free-falling from $y = h \rightarrow -h$ (and hot $\Delta T/2$ plumes ‘free-rising’ from $y = -h \rightarrow h$) in time 2τ at average speed $V = h/\tau$. Using these inertial scalings to estimate the heat flux gives

$$\mathcal{H} \sim V \frac{\Delta T}{2} = \sqrt{g'h} \frac{\Delta T}{2} = \frac{1}{4} \sqrt{g \alpha_v H} (\Delta T)^{3/2} \quad (5)$$

independent of ν and κ , that is

$$Nu = \frac{\mathcal{H}}{\kappa \Delta T/H} \sim \frac{1}{4} \sqrt{Ra Pr}, \quad (6)$$

for the *Nusselt* number $Nu = 1 + \langle vT \rangle / (\kappa \Delta T/H)$ from (4). It has been suggested that (6) characterizes the ‘ultimate state’ of turbulent convection [8], however that conjecture is not supported by recent experiments [9]. Rigorous bounds for no-slip boundary conditions yield $Nu \lesssim 0.0335 Ra^{1/2}$ [10–12] as $Ra \rightarrow \infty$, conflicting with

the free-fall scaling (6) for large Pr . Rigorous bounds for free-slip yield $Nu \lesssim 0.106 Ra^{5/12}$ [13, 14] that conflicts with (6) for any Pr as $Ra \rightarrow \infty$.

A distinct scaling argument is that heat transport is determined by marginal stability of the thermal boundary layers [6, 15]. If δ is the boundary layer thickness, a simple version of this argument assumes $Ra_\delta \equiv g\alpha_\nu(\Delta T/2)\delta^3/(\nu\kappa) \approx Ra_c^{(BL)} \approx 1708/16$ [16], yielding heat flux

$$\mathcal{H} \approx \kappa \frac{\Delta T}{2\delta} \approx \left(\frac{g\alpha_\nu \kappa^2}{16\nu Ra_c^{(BL)}} \right)^{1/3} (\Delta T)^{4/3}, \quad (7)$$

independent of H , that is

$$Nu \sim \frac{Ra^{1/3}}{(16 Ra_c^{(BL)})^{1/3}} \approx 0.084 Ra^{1/3}. \quad (8)$$

We consider 2D flow with $\mathbf{v} = u(x, y, t)\hat{\mathbf{x}} + v(x, y, t)\hat{\mathbf{y}}$. Eliminating p by taking the $\hat{\mathbf{y}}$ component of the curl of the curl of (1) yields

$$\partial_t \nabla^2 v = \nu \nabla^2 \nabla^2 v + \partial_x^2 T + \partial_x (v \nabla^2 u - u \nabla^2 v), \quad (9)$$

$$\partial_t T = \kappa \nabla^2 T - (\mathbf{v} \cdot \nabla) T, \quad (10)$$

$$\partial_t \bar{u} = \nu \partial_y^2 \bar{u} - \partial_y \bar{u} v \quad (11)$$

where ν and κ are now non-dimensionalized by $\sqrt{g'h^3}$ and relate to the Rayleigh and Prandtl numbers as

$$\nu = 4\sqrt{\frac{Pr}{Ra}}, \quad \kappa = \frac{4}{\sqrt{Ra Pr}}. \quad (12)$$

All results in this paper are for $Pr = 7$ (water). The horizontal velocity u is obtained from v and $\partial_x u + \partial_y v = 0$ except for its horizontal average $\bar{u}(y, t)$ that is determined by (11), where the overbar denotes a horizontal average. Equations (9), (10), (11) are considered with no-slip boundary conditions

$$v = \partial_y v = 0, \quad T = \mp 1 \quad \text{at} \quad y = \pm 1, \quad (13)$$

together with periodicity of period $L = 2\pi/\alpha$ in the x direction.

We look for *steady* solutions, $\partial_t = 0$, that bifurcate from the conduction state at $Ra \approx 1708$ for wavenumber $\alpha \approx 3.116/2$ corresponding to aspect ratio $L/H \approx 2.016$. Those convective solutions obey mirror symmetry

$$[u, v, T](x, y) = [-u, v, T](-x, y) \quad (14)$$

as well as shift-reflect symmetry

$$[u, v, T](x, y) = [u, -v, -T](x + \frac{L}{2}, -y). \quad (15)$$

Equations (9), (10) are discretized using a Fourier expansion in x and Chebyshev integration in y [17] with

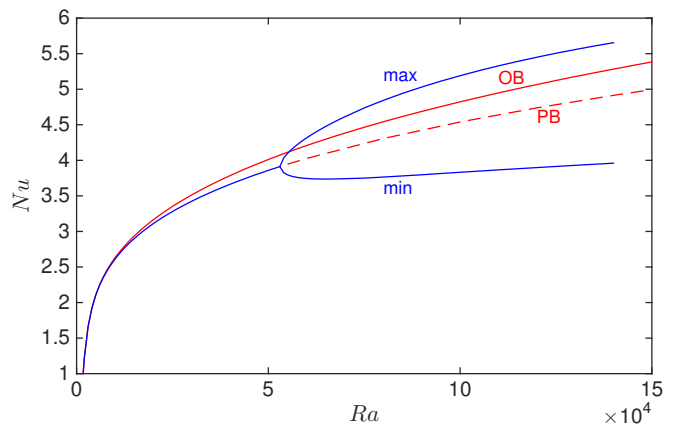


FIG. 1. Nu vs. Ra for steady primary branch (PB) with $L/H = 2$ and optimum branch (OB) bifurcating from conduction state at $Ra = 1708$, $Nu = 1$. Primary branch bifurcates to a time-periodic solution near $Ra = 53000$, max and min Nu achieved by the periodic solution are plotted. Unstable steady state is dashed.

time-marching to steady states. Two distinct codes have been written, code 1 uses the time-accurate scheme in [18], code 2 uses a semi-implicit forward-backward Euler time discretization together with Chebyshev tau of the 2nd kind [19] for the v equation. Code 2 typically uses inconsistent time integration, with smaller time steps for smaller wavenumbers and for the v equation than for the T equation, to speed up or enable convergence to steady state. Both codes are dealiased in x and y . The results of both codes overlap or connect very well (figs. 1, 2, 4). The results also match a 3rd code based on finite differences and a Newton-Krylov iteration to steady state [20]. Mirror symmetry (14) is imposed and eliminates the mean flow (11), but (15) is not imposed explicitly.

We show two branches of nonlinear steady solutions that bifurcate from the conduction state at $Ra \approx 1708$, $\alpha \approx 1.558$. The *primary branch* has fixed horizontal wavenumber α (rounded here to $\alpha = \pi/2 \Leftrightarrow L/H = 2$). The *optimum branch* adjusts α to maximize heat flux Nu . The (Ra, Nu) curves for both solutions are shown in figures 1 and 2. The steady primary solution is stable up to $Ra \approx 53000$ where it spawns a time-periodic solution. The maximum and minimum Nu achieved by that periodic solution are shown in fig. 1, that time periodic solution was computed with the time-accurate code 1. The unstable steady state was continued with code 2 up to $Ra = 5.10^6$ (symbols \circ in fig. 2). Mirror symmetry (14) suffices to stabilize the optimum solution in its fundamental periodic domain. That optimum solution was calculated up to $Ra = 1.4 \cdot 10^6$ with code 1 and $Ra = 10^9$ with code 2 (symbols $*$ in fig. 2). The optimum solution at $Ra = 10^9$ is well-resolved with 200 Chebyshev polynomials in y and 200 Fourier modes in x , after dealiasing.

The heat flux for the unstable primary solution scales

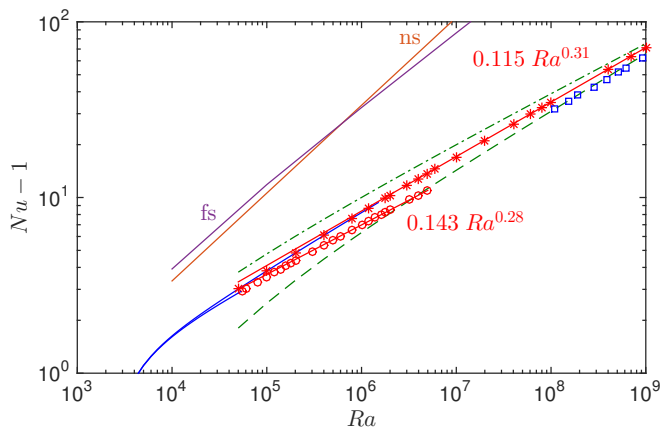


FIG. 2. $Nu - 1$ vs. Ra for primary branch ($\alpha = \pi/2$, red \circ 's) with $Nu - 1 \sim 0.143 Ra^{0.28}$ and optimum branch (red $*$'s) with $Nu - 1 \sim 0.115 Ra^{0.31}$ (least square fit in $10^7 < Ra \leq 10^9$, red solid). Upper dash-dot curve is 3D turbulent data $Nu \sim 0.23 Ra^{0.28}$ from [21] for (outer) aspect ratio 1 and the lower dash is the 3D turbulent data $Nu \sim 0.088 Ra^{0.32}$ from [9] for (outer) aspect ratio 1/2). The blue \square 's for $Ra > 10^8$ is the 'corrected' aspect ratio 4 data in [9, Table 1]. Line 'fs' is the free-slip upper bound $Nu \lesssim 0.106 Ra^{5/12}$ [14]. Line 'ns' is the no-slip upper bound $Nu \lesssim 0.0335 Ra^{1/2}$ [12].

as $Nu - 1 \approx 0.143 Ra^{0.28}$ according to a least square fit in $5 \cdot 10^5 \leq Ra \leq 5 \cdot 10^6$. That solution develops a delicate spiral structure in the temperature field but not in the velocity (fig. 3). The winding of these temperature spirals continuously increases with Rayleigh number. Convergence of our algorithm to that unstable steady solution becomes quite slow for increasing Ra , apparently because of the center region of these spiral structures where $v, T \approx 0$.

The optimum solution increases wavenumber α with Ra as $\alpha \approx 0.133 Ra^{0.217}$ (fig. 4) to achieve an optimum heat flux $Nu - 1 \approx 0.115 Ra^{0.31}$ (fig. 2), from a least square fit in $10^7 < Ra \leq 10^9$. This optimum heat flux scaling is quite similar to the heat flux observed in 3D turbulent convection experiments. Indeed, the optimum branch in fig. 2 is nicely bracketed by the $Nu \approx 0.23 Ra^{0.28}$ data of [21] (in a cylinder of aspect ratio 1) and the $Nu \approx 0.088 Ra^{0.32}$ of [9] (in a cylinder of aspect ratio 1/2). The aspect ratio 4 data [9, Table 1] is well-fitted by $Nu - 1 \approx 0.102 Ra^{0.31}$ in $10^8 \leq Ra \leq 10^{10}$ and lies just below the optimum transport data with $Nu - 1 \approx 0.115 Ra^{0.31}$. This close agreement is remarkable given the differences in dimension, 2D optimum vs. 3D data, and Prandtl number, $Pr = 7$ for the 2D optimum vs. $Pr \approx 0.7$ in the helium gas experiments.

The optimizing wavenumber $\alpha = \alpha^{opt}(Ra)$ (fig. 4) shows an undulation between $1708 < Ra \lesssim 10^6$ that is linked to a temperature spiral structure in the optimum transport solution as well (fig. 5). A temperature up-draft of hot fluid (and downdraft of cold fluid) develops between $Ra = 1708$ and $Ra \approx 10^4$, but a spiral struc-

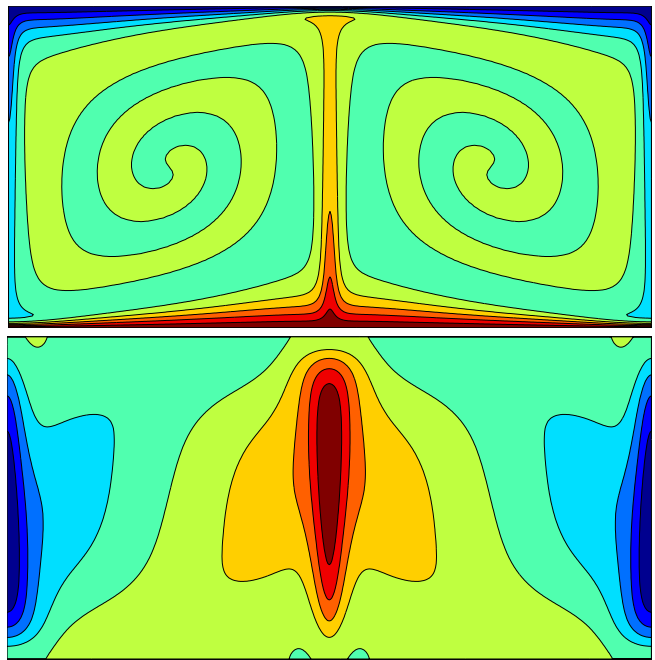


FIG. 3. *Primary solution*. Temperature T (top) and vertical velocity v (bottom) at $Ra = 5 \cdot 10^6$ for $L/H = 2$, $Nu = 11.93$. Equispaced contours at 10% of max-min, actual aspect ratio with $-2 \leq x \leq 2$ horizontal and $-1 \leq y \leq 1$ vertical.

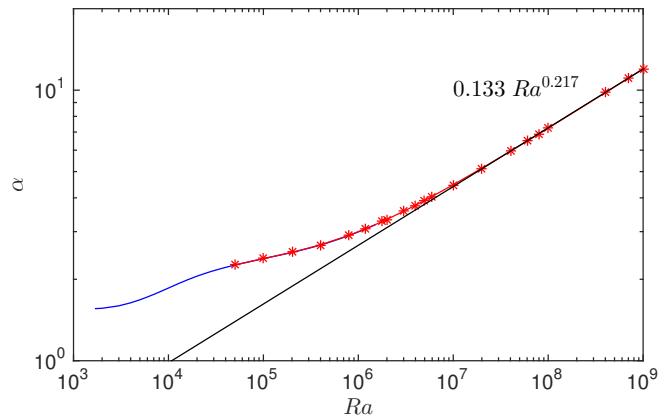


FIG. 4. Horizontal wavenumber $\alpha = \alpha^{opt}(Ra)$ that maximizes heat flux Nu , $\alpha^{opt} \approx 0.133 Ra^{0.217}$ (least square fit in $10^7 < Ra \leq 10^9$).

ture with slight downdraft of warm fluid (and updraft of cool) develops in $10^4 \lesssim Ra \lesssim 10^5$, corresponding to the bump in the curve $\alpha = \alpha^{opt}(Ra)$ in fig. 4. The warm spiral begins winding back up at $Ra \approx 10^5$. The spiral does not appear to ever wind back down for higher Ra , developing instead an increasingly jagged structure (fig. 5, right), and α^{opt} approaches the power law scaling $\alpha^{opt} \approx 0.133 Ra^{0.217}$. The structure of optimum Nu solutions depends on Prandtl number Pr . This is investigated in forthcoming work [20] which also shows that the locally optimum steady solution discussed here is in

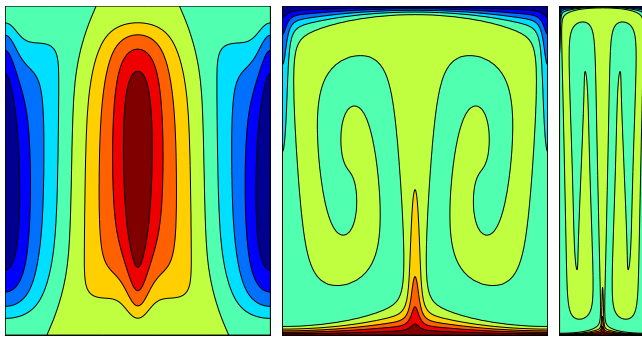


FIG. 5. *Optimum solution.* Velocity v (left) and temperature T (center) at $Ra = 5 \cdot 10^6$, $L/H = 0.803$, $Nu = 14.72$. Temperature T (right) at $Ra = 10^9$, $L/H = 0.262$, $Nu = 72.3$. Equispaced contours at 10% of max-min, actual aspect ratio.

fact the global optimum over α .

The close agreement between the optimum transport 2D steady state solutions and 3D turbulent data in fig. 2 is intriguing. Although this agreement could be fortuitous, it strongly suggests that a single unstable steady solution may capture key statistical features of fully developed turbulent flows, such as the net heat flux and the mean temperature profile as well as the strength and scale of elemental plumes, as in shear flows [17, 22]. A search for such maximum momentum transport solutions in shear flows was initiated over 10 years ago but not completed because of the higher computational complexity of those 3D solutions (J. Wang and F. Waleffe, 2004, unpublished).

Our results are connected with Malkus' theory of turbulent convection [6] and subsequent work on upper bounds [10–14]. Two key ingredients of Malkus' theory are maximum heat transport and marginal stability of the mean temperature profile and the smallest scales of motion. Both ingredients are included in our calculations that maximize heat transport over horizontal wavenumber α and track steady state solutions that bifurcate from the marginal stability critical point at $Ra \approx 1708$, $\alpha \approx 1.558$. We conjecture that our 2D results are in fact the 3D optimum transport solutions (for infinite or periodic horizontal directions). Whether the ultimate scaling of these optimum solutions is $Nu \sim Ra^{1/3}$ as $Ra \rightarrow \infty$ remains to be seen but is possible.

Why the optimum transport solution should capture gross 3D turbulence characteristics might be understood as a 'winner-take-all' effect, where the optimum solution consumes all available potential energy so no other flow can be sustained. The optimum solution appears to be stable when mirror symmetry (14) is imposed and length scales are restricted to be less or equal to the optimum wavelength. The optimum solution is unstable to larger scale perturbations, in particular to subharmonics

where plumes merge and form bigger plumes in a cyclic or quasi-cyclic fashion. It is also unstable to a mean shear flow (11) when mirror symmetry is allowed to be broken. These instabilities would be the source of the 'turbulence' but the underlying unstable coherent solutions control the heat transport.

The authors would like to thank Charles Doering (U Michigan) and David Sondak (UW Madison) for helpful comments and discussions. This research was partially supported by NSF grants DMS-0807349 (FW, AB) and DMS-1008396 (AB, LMS).

* waleffe@math.wisc.edu

- [1] E. N. Lorenz, *Journal of Atmospheric Sciences*, **20**, 130 (1963).
- [2] A. Libchaber, C. Laroche, and S. Fauve, *Journal de Physique Lettres*, **43**, 211 (1982).
- [3] E. Bodenschatz, W. Pesch, and G. Ahlers, *Annual Review of Fluid Mechanics*, **32**, 709 (2000).
- [4] G. Ahlers, S. Grossmann, and D. Lohse, *Reviews of Modern Physics*, **81**, 503 (2009).
- [5] M. A. Dominguez-Lerma, G. Ahlers, and D. S. Cannell, *Physics of Fluids (1958-1988)*, **27**, 856 (1984).
- [6] W. V. Malkus, *Proceedings of the Royal Society of London. Series A. Mathematical and Physical Sciences.*, **225**, 196 (1954).
- [7] The physical heat flux is $\rho_0 C_p \mathcal{H}$ where C_p is the specific heat capacity a constant pressure.
- [8] E. A. Spiegel, *Annual Review of Astronomy and Astrophysics*, **9**, 323 (1971).
- [9] J. Niemela and K. R. Sreenivasan, *Journal of fluid mechanics*, **557**, 411 (2006).
- [10] F. H. Busse, *Journal of Fluid Mechanics*, **37**, 457 (1969).
- [11] C. R. Doering and P. Constantin, *Physical Review E*, **53**, 5957 (1996).
- [12] R. R. Kerswell, *Physics of Fluids*, **13**, 192 (2001).
- [13] J. P. Whitehead and C. R. Doering, *Physical Review Letters*, **106**, 244501 (2011).
- [14] B. Wen, G. Chini, R. R. Kerswell, and C. R. Doering, submitted to *Physics Letters A* (2015).
- [15] L. N. Howard, in *Applied Mechanics*, edited by H. Görtler (Springer, 1966) pp. 1109–1115.
- [16] Estimated from linear stability about the conduction state but with free 'outflow' boundary conditions at the top edge of the boundary layer, that is $\partial_y v = \partial_y^3 v = \partial_y(T + y) = 0$.
- [17] F. Waleffe, *Phys. Fluids*, **15**, 1517 (2003).
- [18] P. R. Spalart, R. D. Moser, and M. M. Rogers, *Journal of Computational Physics*, **96**, 297 (1991).
- [19] M. Charalambides and F. Waleffe, *SIAM Journal on Numerical Analysis*, **47**, 48 (2008).
- [20] D. Sondak, L. M. Smith, and F. Waleffe, *Journal of Fluid Mechanics (to be submitted)* (2015).
- [21] B. Castaing, G. Gunaratne, F. Heslot, L. Kadanoff, A. Libchaber, S. Thomae, X.-Z. Wu, S. Zaleski, and G. Zanetti, *Journal of Fluid Mechanics*, **204**, 1 (1989).
- [22] G. Kawahara, M. Uhlmann, and L. van Veen, *Annual Review of Fluid Mechanics*, **44**, 203 (2012).